Chlorination Strategy Induced Abnormal Nanomorphology Tuning in High Efficiency Organic Solar Cells – A Study of Phenyl Substituted Benzodithiophene Based Non-Fullerene Acceptors

*Cenqi Yan, Tao Yang , Wei Gao , Yiqun Xiao, Yuhao Li, Xinhui Lu, Chuluo Yang, and Gang Li**

Dr. Cenqi Yan, Prof. Gang Li,
Department of Electronic and Information Engineering, The Hong Kong Polytechnic University, Hong Hum, Kowloon, Hong Kong, China. E-mail addresses: gang.w.li@polyu.edu.hk

Prof. Tao Yang
Key Laboratory of Biofuels, Qingdao Institute of Bioenergy and Bioprocess Technology, Chinese Academy of Sciences, 266101, China.

Dr.Wei Gao, Prof. Chuluo Yang
Hubei Key Lab on Organic and Polymeric Optoelectronic Materials, Department of Chemistry, Wuhan University, Wuhan, 430072, China.
Shenzhen Key Laboratory of Polymer Science and Technology, College of Materials Science and Engineering, Shenzhen University, Shenzhen, 518060, China.

Yiqun Xiao, Yuhao Li, Prof. Xinhui Lu
Department of Physics, Chinese University of Hong Kong, New Territories, Hong Kong, China.

Abstract: A new heptacyclic core based on phenyl substituted Benzo[1,2-b:4,5-b']dithiophene (BDT) is designed, and paired with 1,1-dicyano methylene-3-indanone (INCN) end group to construct a non-fullerene acceptor, BPIC. The strong aggregation and large phase separation in PBDB-T:BPIC blend cause inefficient exciton dissociation and ineffective charge transport, resulting in a low 11.12% power conversion efficiency (PCE) with the low short-circuit current density (J_{SC}), and fill factor (FF). To finely control the active-layer nanomorphology, the chlorine atom is introduced into the INCN termini, and di-chlorinated BPIC-2Cl and tetra-chlorinated BPIC-4Cl are synthesized. It is an interesting phenomenon that, unlike other literature reports, while the di-chlorination reduces crystallinity and phase-separation scale, further chlorination increases crystallinity and phase separation. PBDB-T:BPIC-2Cl device exhibits suitable molecular packing and nearly ideal nanoscale phase separation, which facilitates exciton dissociation and charge transport and thus yields the higher PCE of 12.63% with significantly improved J_{SC} and FF. PBDB-T:BPIC-4Cl device, however, exhibits strong stacking intensity and excessively large phase separation, leading to the obviously reduced J_{SC}, FF and PCE of only 8.23%. This work demonstrates that novel phenyl substituted BDT core and delicated chlorination strategy provides powerful tools for high-performance non-fullerene acceptors in OSCs.

Keywords: phenyl substitution, chlorination, morphology, non-fullerene acceptor, organic solar cells

1. Introduction

Non-fullerene acceptors (NFAs) [1-4] are currently a major focus of research in the development of bulk-heterojunction organic solar cells (OSCs).[5-7] Compared with the widely used fullerene acceptors, [8-10] NFAs offer the advantages of easy modification of chemical structures and electronic energy levels, strong absorption in the visible and near-infrared region, coupled with good stability.[11, 12] Recent developments have led to a rapid increase in power conversion efficiencies (PCEs) of NFA OSCs to ~ 16%, not only demonstrating the viability of using NFAs to replace fullerene acceptors, [13-19] but also encouraging OSC commercial future.

Fused-ring electron acceptors (FREAs), as an important class of non-fullerene acceptors, typically consist of electron-donating planar fused ring flanked with two strong electron-withdrawing end groups,[20] substituted by side chains.[21-25] A majority of FREAs, including the representative IDIC and ITIC, utilized extended fused-ring indacenodithiophene (IDT) or indacenodithieno [3, 2-*b*] thiophene (IDTT) as the central building block. [26-30] Benzo[1,2-b:4,5-b′]dithiophene (BDT) unit is a rather widely used building block in donors, partially due to its symmetric and planar conjugated structure. [31-40] For instance, polymeric donor PBT1-C[41] with alkylphenyl substituted BDT core, demonstrated a record high fill factor of 80.5% in fullerene OSCs and showed a good efficiency of 12.7% with a very high fill factor of 78.5% in ITCPTC based OSCs, due to the formation of optimal interpenetrating network nanomorphology. FREAs based on phenyl substituted BDT has never been demonstrated, despite the report of alkyl[42]/thiophene[43-45] substitution of BDT central unit. On the other side, electron-withdrawing end groups also have important influences in the properties of fused-ring electron acceptors. The “acceptor-donor-acceptor” structure can induce intramolecular charge transfer (ICT), tune the lowest unoccupied molecular orbital (LUMO) and highest occupied molecular orbital (HOMO) energy levels, and

lead to broad and strong absorption. Further chlorination of end groups can strengthen ICT effect, reduce LUMO and HOMO, and expand absorption throughout the visible and even near-infrared region. And typically, chlorination enhance π-π stacking and crystallinity.[46-48] For example, in the system of PBDB-T:IXIC, chlorination enhanced π-π stacking and crystallinity, and gradually reduced the average domain size from 31.96 nm, to 25.20 nm in PBDB-T:IXIC-2Cl and 23.53 nm in PBDB-T:IXIC-4Cl. For the all-small-molecule system of DRCN5T and F-0Cl, chlorination by 2-Cl and 4-Cl monotonically increased π-π stacking, crystallinity, and domain size.

Herein, we designed and synthesized a new heptacyclic core based on phenyl substituted BDT, and constructed a non-fullerene acceptor, BPIC, by pairing the new core with 1,1-dicyano methylene-3-indanone (INCN) termini. The strong aggregation and large phase separation observed in PBDB-T:BPIC blend, caused inefficient exciton dissociation and ineffective charge transport, resulting in the PCE of 11.12% with the low short-circuit current density (J_{SC}), and the low fill factor (FF). To finely optimize the active-layer morphology, we introduced the chlorine atom into the INCN termini. We found an interesting new phenomenon that, the di-chlorination reduced crystalline intensity and phase-separation scale, while further chlorination (4-Cl) increased crystallinity and phase separation instead. This non-monotonic change was observed for the first time. The PBDB-T:BPIC-2Cl device exhibited suitable stacking intensity and nearly ideal phase separation, which facilitated exciton dissociation and charge transport, and thus afforded the high PCE of 12.63% with significantly improved J_{SC} and FF. In contrast, the PBDB-T:BPIC-4Cl system exhibited strong stacking intensity and excessive phase separation, leading to obviously reduced J_{SC}, FF and a poor PCE of 8.23%.

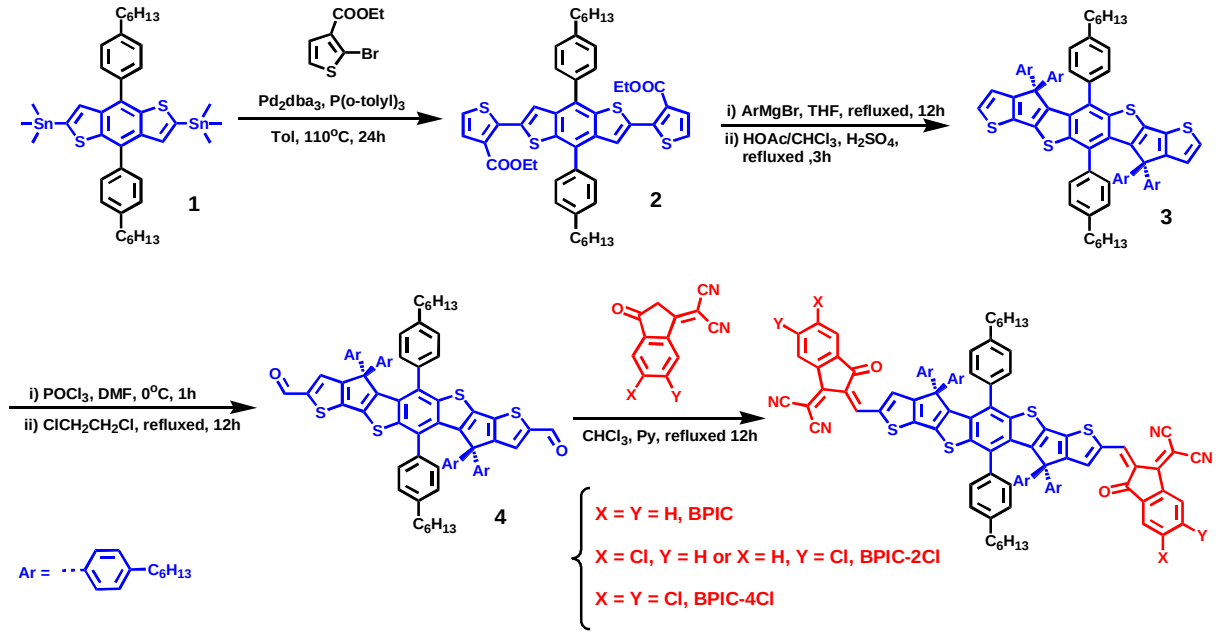

Scheme 1 Synthetic Routes to BPIC, BPIC-2Cl and BPIC-4Cl.

2. Results and discussion

2.1 Synthesis and characterization

The synthetic routes to BPIC, BPIC-2Cl and BPIC-4Cl were illustrated in **Scheme 1**. BPIC, BPIC-2Cl and BPIC-4Cl were characterized by mass spectrometry, ^{1}H NMR, ^{13}C NMR and elemental analysis (see ESI). BPIC, BPIC-2Cl and BPIC-4Cl had good solubility in common organic solvents such as chloroform, chlorobenzene and *o*-dichlorobenzene at room temperature.

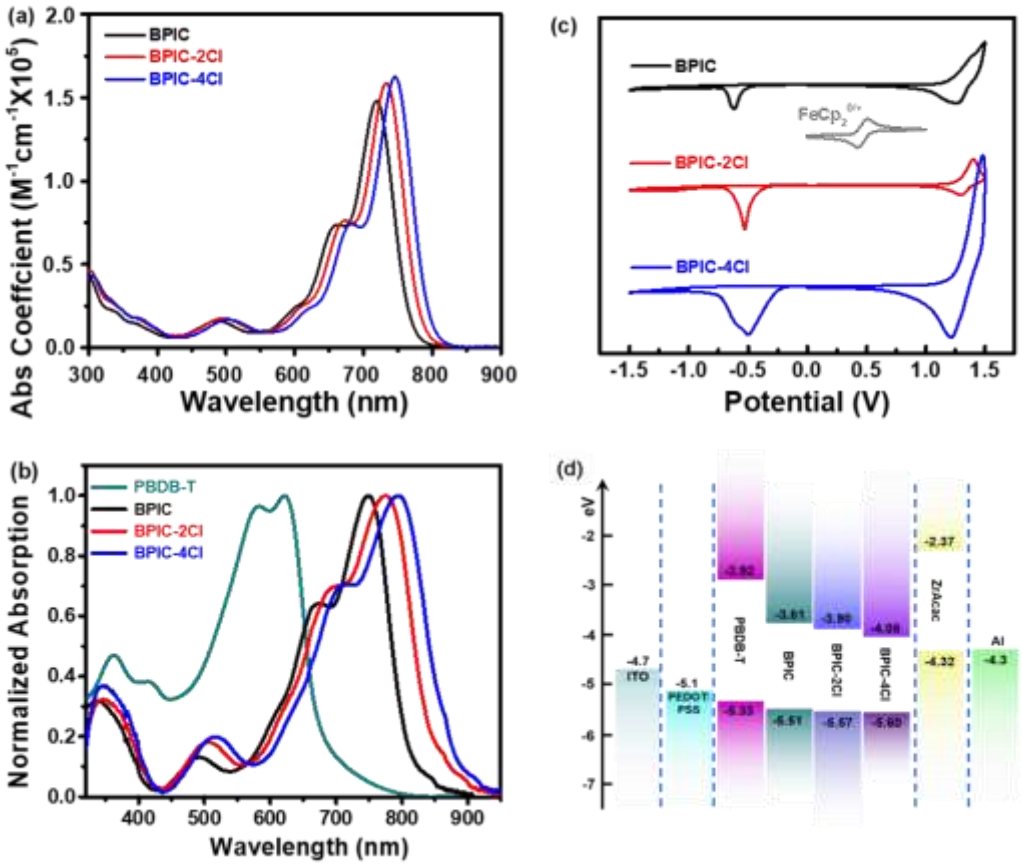

Figure 1 (a) UV-vis absorption spectra of BPIC, BPIC-2Cl and BPIC-4Cl in chloroform solution (10^{-6} M). (b) UV-vis absorption spectra of PBDB-T, BPIC, BPIC-2Cl and BPIC-4Cl pure films. (c) Cyclic voltammograms for BPIC, BPIC-2Cl and BPIC-4Cl. (d) Energy level diagram of the layers of the device.

The optical absorption spectra of BPIC, BPIC-2Cl and BPIC-4Cl in chloroform solution (10^{-6} M) and thin films were shown in **Figure 1a** and **1b**, respectively. BPIC showed an absorption maximum at 719 nm with a molar absorptivity of 1.48×10^5 M^{-1} cm^{-1} in solution. Di-chlorination and Tetra-chlorination red-shifted and slightly improved light absorption. Compared with BPIC, BPIC-2Cl and BPIC-4Cl displayed absorption maxima at 733 and 746 nm in solution, with molar absorptivity of 1.59×10^5 and 1.62×10^5 M^{-1} cm^{-1}, respectively. The absorption maxima of BPIC, BPIC-2Cl and BPIC-4Cl films are at 749, 775 and 795 nm, red-shifted 30, 42 and 49 nm relative

to those in solution, respectively. With the increasing extent of chlorination, the optical band gaps narrowed from 1.53 eV for BPIC to 1.47 eV for BPIC-2Cl and 1.43 eV for BPIC-4Cl. (**Table 1**). Cyclic voltammetry (CV) measurements were performed to investigate the electronic energy levels of BPIC, BPIC-2Cl and BPIC-4Cl (**Figure 1c**). All these acceptors exhibited irreversible reduction waves and oxidation waves. The highest occupied molecular orbital (HOMO) and the lowest unoccupied molecular orbital (LUMO) energy levels are estimated from the onset oxidation and reduction potentials, respectively. Non-chlorinated BPIC exhibited a HOMO of −5.51 eV and a LUMO of −3.81 eV. BPIC-2Cl and BPIC-4Cl presented HOMO/LUMO energy levels of −5.57/−3.90 and −5.60/−4.08 eV, respectively (**Figure 1d** and **Table 1**). The chlorination of INCN end groups obviously down-shifted HOMO and LUMO, due to the electron-withdrawing property of chlorine.

Table 1 Basic properties of BPIC, BPIC-2Cl and BPIC-4Cl.

Compound	λ_{max} (nm)		E_g^{opt} [a]	ε [b]	E_{ox}/E_{red} (V) [c]	HOMO [c]	LUMO [c]	μ_e
	solution	film	(eV)	(M^{-1} cm^{-1})		(eV)	(eV)	(cm^2 V^{-1} s^{-1})
BPIC	719	749	1.53	1.48×10^5	1.18/−0.52	−5.51	−3.81	6.34×10^{-4}
BPIC-2Cl	733	775	1.47	1.59×10^5	1.23/−0.43	−5.57	−3.90	7.08×10^{-4}
BPIC-4Cl	746	795	1.43	1.62×10^5	1.26/−0.25	−5.60	−4.08	5.68×10^{-4}

[a] Estimated from the absorption edge in film; [b] Molar absorptivity at λ_{max} in solution; [c] Estimated from Cyclic voltammetry (CV) method by measuring film in acetonitrile.

2.2 Photovoltaic properties

The previously reported wide-bandgap polymer donor PBDB-T[49] (**Scheme 1**) possessed strong absorption from 350 to 750 nm, which complements those of low-bandgap BPIC, BPIC-2Cl and BPIC-4Cl (**Figure 1a**). The energy levels of PBDB-T (HOMO = −5.33 eV; LUMO = −2.92 eV) matched well with those acceptors, beneficial to efficient exciton dissociation, and its deep HOMO

energy level favored high open-circuit voltage (V_{OC}). We fabricated BHJ OSCs with a device structure of indium tin oxide (ITO)/ poly(3,4-ethylenedioxythiophene):poly(styrene sulfonate) (PEDOT:PSS)/ PBDB-T:acceptor/ zirconium acetylacetonate (Zracac) [50]/Al (**Scheme S1**). The optimal donor: acceptor weight ratio is 1:1. **Table 2** summarized the V_{OC}, J_{SC}, FF, and PCE of the optimized devices. The current density-voltage (*J*-*V*) curves of the best devices were shown in **Figure 2a**. The average V_{OC} gradually descended with the increasing extent of chlorination, from 0.880 V for BPIC to 0.814 V for BPIC-2Cl and 0.742 V for BPIC-4Cl, in accord with the down-shift trend of LUMO values of the acceptors (Table 1). The average J_{SC} and FF displayed non-monotonic change and reached maximum in PBDB-T:BPIC-2Cl device, leading to the higher average PCE of 12.20%, despite the middling V_{OC} of 0.814 V. The champion PBDB-T:BPIC-2Cl device demonstrated a PCE_{max} of 12.63% with a V_{OC} of 0.822 V, a J_{SC} of 21.08 mA cm^{-2} and a FF of 72.9%, outperforming those of BPIC and BPIC-4Cl (PCE_{max} of 11.12% and 8.23%).

Table 2 Photovoltaic performance and mobilities of the optimized devices based on PBDB-T: acceptor.

device[a)]	V_{OC}[b)] (V)	J_{SC}[b)] (mA cm^{-2})	calc. J_{SC} (mA cm^{-2})	FF[b)] (%)	PCE[b)] (%)	μ_h (cm^2 V^{-1} s^{-1})	μ_e (cm^2 V^{-1} s^{-1})	μ_h/μ_e
PBDB-T: BPIC	0.880±0.005 (0.886)	17.92±0.21 (18.23)	17.92	68.1±1.0 (68.8)	10.74±0.28 (11.12)	7.35×10^{-4}	3.82×10^{-4}	1.92
PBDB-T: BPIC-2Cl	0.814±0.008 (0.822)	20.73±0.28 (21.08)	20.45	72.3±0.7 (72.9)	12.20±0.30 (12.63)	7.54×10^{-4}	4.43×10^{-4}	1.70
PBDB-T: BPIC-4Cl	0.742±0.006 (0.749)	17.11±0.21 (17.21)	16.72	63.1±1.1 (63.8)	8.01±0.22 (8.23)	7.12×10^{-4}	3.43×10^{-4}	2.08

[a)] PBDB-T: acceptor = 1:1 (w/w); [b)] Average values with standard deviation were obtained from 20 devices; the values in parentheses are the parameters of the best device.

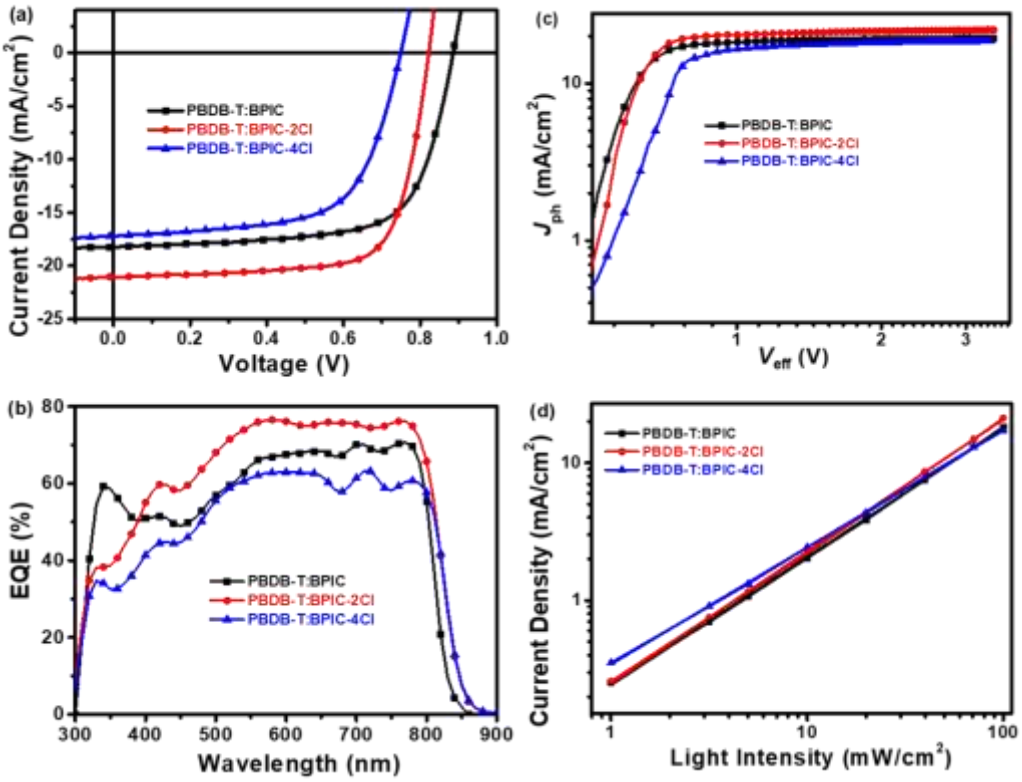

Figure 2 (a) Current density-voltage (*J*-*V*) curves, (b) EQE spectra, (c) J_{ph} versus V_{eff} and (d) J_{sc} versus P_{light} of the optimized devices with the structure of ITO /PEDOT:PSS /PBDB-T:acceptor/Zracac/Al.

The external quantum efficiency (EQE) spectra of the optimized devices were shown in **Figure 2b**. Compared with non-chlorinated BPIC, chlorinated BPIC-2Cl and BPIC-4Cl exhibited broader EQE response in PBDB-T based devices, consistent with the broad and red-shifted absorption of the latter two acceptors. The EQE maxima of PBDB-T: BPIC, PBDB-T: BPIC-2Cl, and PBDB-T: BPIC-4Cl blends are 70.7%, 76.1%, and 63.2%, respectively. The J_{SC} of PBDB-T: BPIC, PBDB-T: BPIC-2Cl, and PBDB-T: BPIC-4Cl blends calculated from integration of EQE spectra with the AM 1.5G reference spectrum are 17.92, 20.45, and 16.72 mA cm^{-2}, respectively, consistent with J_{SC} values measured from *J*−*V* curves (the error is < 3%, **Table 2**).

We measured the photocurrent density (J_{ph}) versus the effective voltage (V_{eff}) to investigate the charge generation and extraction properties (**Figure 2c**). At high V_{eff} of 3 V, all the photogenerated excitons are assumed to be dissociated into free charge carriers and collected by electrodes[51]. PBDB-T: BPIC-2Cl device presented a J_{sat} of 21.92 mA cm^{-2}, much higher than that of the PBDB-T: BPIC (19.34 mA cm^{-2}) and PBDB-T: BPIC-4Cl device (18.60 mA cm^{-2}), which meant PBDB-T: BPIC-2Cl blend have better light absorption. The exciton dissociation efficiency ($\eta_{diss} = J_{SC}/J_{sat}$) and charge collection efficiency ($\eta_{coll} = J_{max}/J_{sat}$) were calculated under the short circuit and maximum power output conditions, respectively. The PBDB-T: BPIC-2Cl device revealed a η_{diss} of 96.1% and a η_{coll} of 83.4%, both higher than those of PBDB-T: BPIC (η_{diss} of 94.3% and η_{coll} of 78.6%) and PBDB-T: BPIC-4Cl (η_{diss} of 92.5% and η_{coll} of 75.0%), indicative of more efficient exciton dissociation and charge transport.

Charge recombination in the devices was investigated by measuring J_{SC} with different incident light intensities (P_{light}) (**Figure 2d**). The relationship between J_{SC} and P_{light} can be described by the formula $J_{SC} \propto P^S$; S = 1 indicates all free carriers are swept out and collected at the electrodes prior to recombination, while S < 1 indicates the existence of bimolecular recombination. PBDB-T: BPIC-2Cl device displayed an S value of 0.96, slightly surpassing that of PBDB-T: BPIC (0.93) and obviously exceeding that of PBDB-T: BPIC-4Cl counterparts (0.85). The weakest bimolecular recombination in PBDB-T: BPIC-2Cl device corresponded with the highest η_{coll} of 83.4% and the highest FF of 72.9%.

The electron mobilities of pure acceptor films and the blended films, and the hole mobilities of the blended films were measured by the space charge limited current (SCLC) method (**Figure S13** and **S14**). [52] BPIC-2Cl displayed a slightly higher electron mobility than BPIC and BPIC-4Cl. The hole and electron mobilities of PBDB-T: BPIC-2Cl blends are 7.54×10^{-4} and 4.43×10^{-4} cm^2

V^{-1} s^{-1}, respectively, higher than those of PBDB-T: BPIC (7.35×10^{-4} and 3.82×10^{-4} cm^2 V^{-1} s^{-1}) and PBDB-T: BPIC-4Cl blend (7.12×10^{-4} and 3.43×10^{-4} cm^2 V^{-1} s^{-1}). The higher and more balanced charge mobilities (μ_h/μ_e = 1.70) in PBDB-T: BPIC-2Cl blend accounted for its weaker bimolecular recombination, more efficient charge extraction and higher FF of 72.9%. [53]

2.3 Film morphology

Atomic force microscopy (AFM) was used to detect surface roughness and phase separation. Grazing-incidence wide-angle X-ray scattering (GIWAXS) and grazing incidence small angle X-ray scattering (GISAXS) were adopted to investigate molecular packing and nanoscale phase separation in thin films. [54, 55]

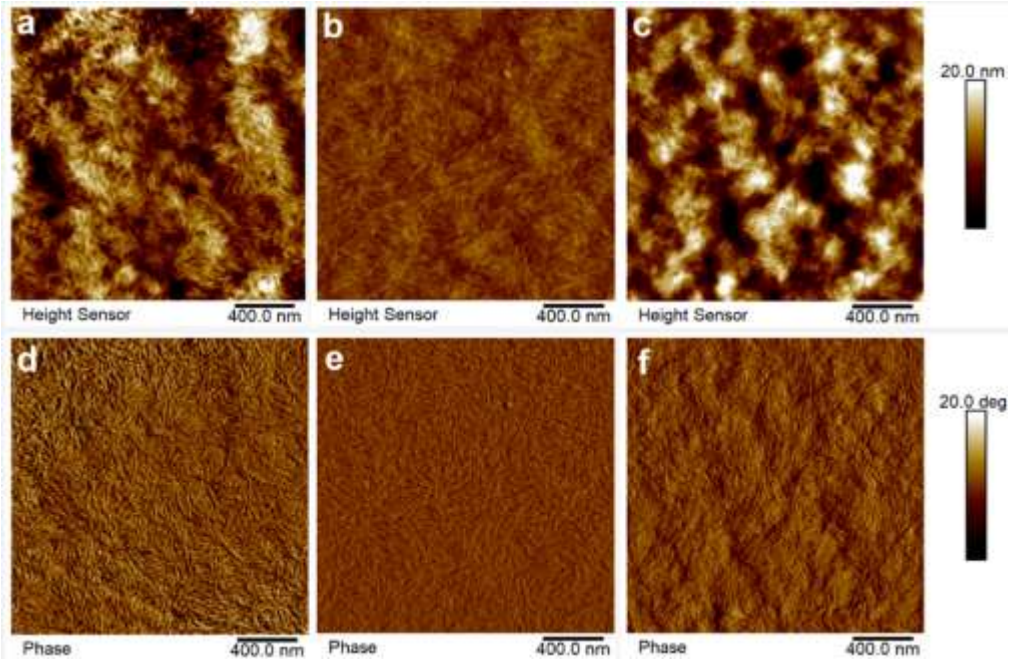

Figure 4 AFM height images (a-c) and phase images (d-f) of (a,d) PBDB-T:BPIC, (b,e) PBDB-T:BPIC-2Cl and (c,f) PBDB-T:BPIC-4Cl blends. (scale bar: 400 nm)

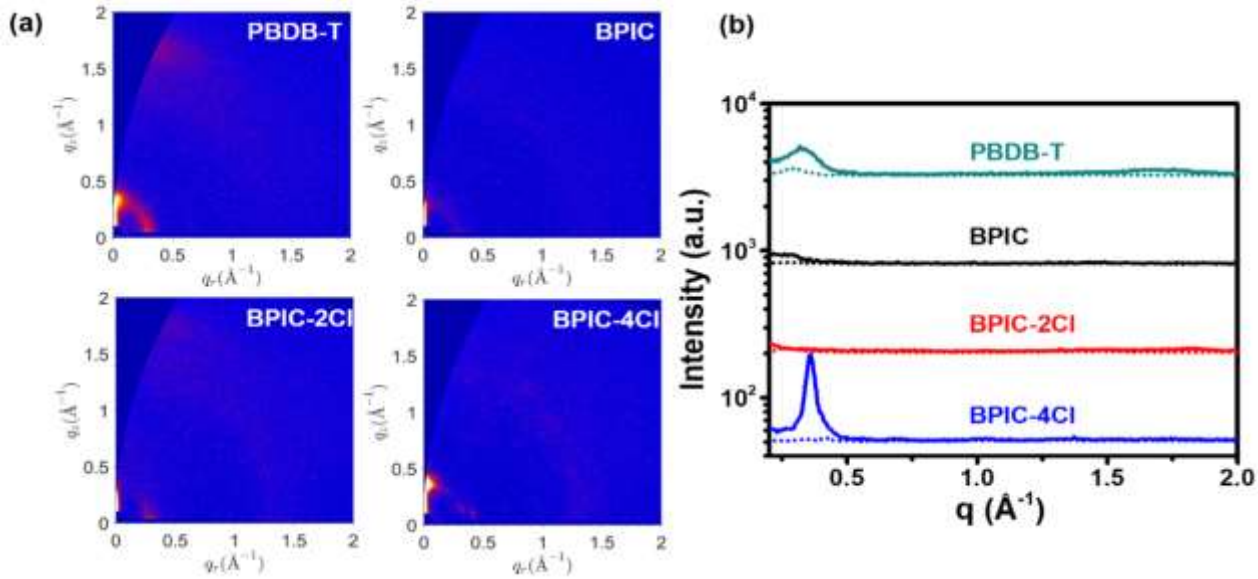

Figure 5 (a) 2D GIWAXS patterns of PBDB-T, BPIC, BPIC-2Cl and BPIC-4Cl neat films, and (b) the corresponding GIWAXS intensity profiles along the in-plane (dashed lines) and out-of-plane (solid lines) directions.

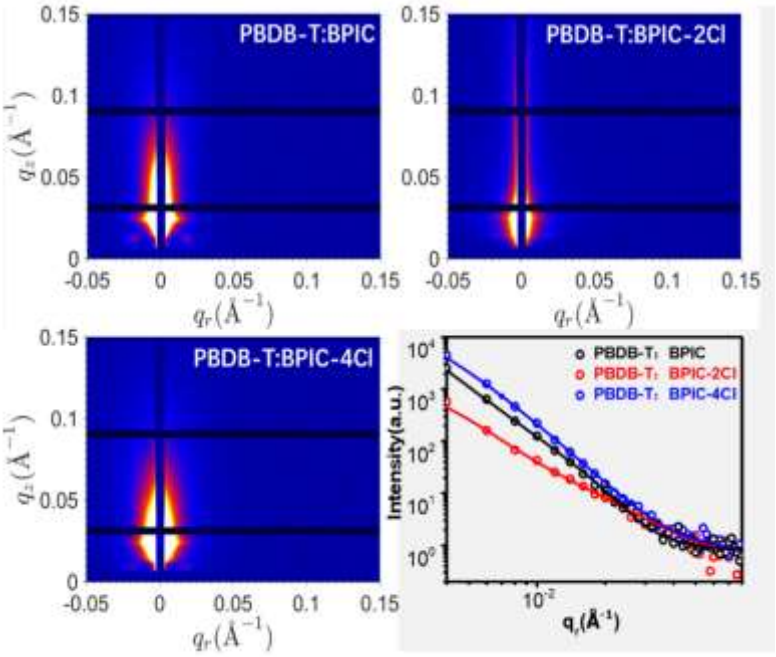

Figure 6 2D GISAXS patterns of PBDB-T: BPIC, PBDB-T: BPIC-2Cl and PBDB-T: BPIC-4Cl blends and the intensity profiles and best fittings along the in-plane direction.

As shown in AFM height images (**Figure 4**), PBDB-T: BPIC-2Cl blend exhibited a root mean square roughness (R_q) of 1.04 nm, obviously smaller than that of PBDB-T: BPIC (3.41 nm) and PBDB-T: BPIC-4Cl (4.01 nm), which perfectly fitted the stacking intensity revealed in the GIWAXS data of donor:acceptor blend. **Figure S15** presented two-dimensional (2D) GIWAXS patterns of PBDB-T: BPIC, PBDB-T: BPIC-2Cl and PBDB-T: BPIC-4Cl blend films and the corresponding intensity profiles along in-plane and out-of-plane directions. PBDB-T: BPIC blended films exhibited two π-π peaks and very strong lamellar peaks in the out-of-plane direction. According to the GIWAXS data of pure film (**Figure 5**), the π-π peak at larger $q_z \approx 1.72$ Å^{-1} with crystalline correlation length (CCL) of 35.3 Å possibly belonged to BPIC, while the π-π peak at smaller $q_z \approx 1.53$ Å^{-1} with CCL of 36.2 Å may originated from PBDB-T, implying large-scale phase separation in PBDB-T: BPIC blend. Along the out-of-plane direction, PBDB-T: BPIC-2Cl blend exhibited π-π peaks at $q_z \approx 1.74$ Å^{-1} with CCL of 16.7 Å, while PBDB-T: BPIC-4Cl blend displayed an increased CCL of 20.7 Å for π-π peaks at $q_z \approx 1.74$ Å^{-1}. The smoother film surface and suitable stacking intensity are favorable for interface contact and charge collection. **Figure 5** presented two-dimensional (2D) GIWAXS patterns of PBDB-T, BPIC, BPIC-2Cl and BPIC-4Cl pure films. PBDB-T neat film exhibited bimodal lamellar peaks ($q_r \approx 0.29$ Å^{-1}, d ≈ 21.66 Å and $q_z \approx 0.32$ Å^{-1}, d ≈ 19.63 Å) and the π-π peaks ($q_z \approx 1.69$ Å^{-1}, d ≈ 3.71 Å). BPIC neat films barely showed any scattering peaks, demonstrating an amorphous nature. By contrast, BPIC-2Cl exhibited a preferential "face-on"-oriented packing with the π-π peak at $q_z \approx 1.82$ Å^{-1} (d ≈ 3.45 Å). In contrast, BPIC-4Cl demonstrated a strong edge-on structural ordering with a sharp lamellar peak at $q_z \approx 0.36$ Å^{-1} (d ≈ 17.4 Å, CCL= 157.3 Å^{-1}). The proposed chlorination strategy here could effectively influence the molecular packing of acceptors.

Figure 6 presented 2D GISAXS patterns of PBDB-T: BPIC, PBDB-T: BPIC-2Cl and PBDB-T: BPIC-4Cl blends, and the intensity profiles and best fittings along the in-plane direction. The data were fitted with fractal-like network models and Debye-Anderson-Brumberger (DAB) models, to account for the scattering contribution from pure phase domains and the intermixing amorphous phase, respectively. PBDB-T:BPIC-2Cl exhibited an pure phase domain size (2Rg) of 23.2 nm, very close to the exciton diffusion length, which would allow efficient exciton dissociation. In contrast, PBDB-T:BPIC and PBDB-T:BPIC-4Cl exhibited excessively large pure phase domain sizes of 47.1 and 99.1 nm. The corresponding correlation lengths of the amorphous intermixed phases were fitted to be 59.1, 29.5 and 39.4 nm, for PBDB-T:BPIC, PBDB-T:BPIC-2Cl and PBDB-T:BPIC-4Cl blend, respectively. The smallest intermixing phase for the PBDB-T:BPIC-2Cl blend film was well consistent with the results observed in AFM phase images (**Figure 4**). PBDB-T: BPIC-2Cl blend showed more uniform and finer nanofibrillar network than PBDB-T: BPIC and PBDB-T: BPIC-4Cl. The smaller aggregated domains of BPIC-2Cl based blend led to a larger donor/acceptor interfacial area, which was favorable for exciton dissociation, and the interpenetrating network therein facilitated hole and electron transport. The nearly ideal phase separation scale and fine nanofibrillar network accounted for the higher η_{diss}, η_{coll}, *J*sc, FF, and efficiency of PBDB-T: BPIC-2Cl system.

Evidenced in AFM, GIWAXS and GISAXS, the di-chlorination reduced crystalline intensity and phase-separation scale while further chlorination (4-Cl) increased crystallinity and phase separation obviously. This non-monotonic change with different degree of chlorination is very different from the reported NFA chlorination works in the past literature. For example, for the system of PBDB-T:IXIC, chlorination enhanced π-π stacking and crystallinity, and monotonically reduced the average domain size from 31.96 nm without Cl, to 25.20 nm in PBDB-T:IXIC-2Cl

and 23.53 nm in PBDB-T:IXIC-4Cl. On the other hand, for the all-small-molecule system of DRCN5T:F-0Cl, chlorination gradually increased not only π-π stacking, crystallinity, but also the domain size, all in monotonic manner. The non-monotonic morphology tuning trend by controlling the degree of NFA chlorination in this manuscript provides a novel way of improving NFA OSC morphology and performance.

3. Conclusions

To summarize, by combining a new phenyl-substituted-BDT based heptacyclic core with two INCN termini, we first designed a new non-fullerene acceptor, BPIC. The PBDB-T:BPIC device suffered strong aggregation and large phase separation with limited PCE of 11.12%, due to inefficient exciton dissociation and ineffective charge collection. Chlorination of the INCN termini in BPIC led to BPIC-2Cl and BPIC-4Cl NFAs, in which we observed interesting non-monotonic morphology tuning trend. Di-chlorination reduced crystalline intensity and phase-separation, while tetra-chlorination showed clearly increased crystallinity and phase separation comparing to the di-chlorination case, which has never been reported before. This new phenomenon allowed us to achieve suitable molecular packing and nearly ideal phase separation in PBDB-T:BPIC-2Cl device, which facilitated exciton dissociation and charge transport, and a high PCE of 12.63%. The PBDB-T:BPIC-4Cl system, however, exhibited excessively large crystallization and phase separation, leading to poor PCE of 8.23%. These results offered more insight into the understanding of the champion photovoltaic performance of PBDB-T:BPIC-2Cl blend, which will benefit future design of high-performance non-fullerene acceptors.

Supporting information

Supporting Information is available from the Wiley Online Library or from the author.

Acknowledgments

G. Li thanks the support from Research Grants Council of Hong Kong (Project Nos 15218517, C5037-18G), Shenzhen Science and Technology Innovation Commission (Project No. JCYJ20170413154602102), and the funding for Project of Strategic Importance provided by the Hong Kong Polytechnic University (Project Code: 1-ZE29). T.Y. thanks the financial support from the Science and Technology Commission of the Military Commission of China (NO. 18-H863-00-TS-002-006-01). C-L. Y. thanks the National Natural Science Foundation of China (No. 21572171).

Received: ((will be filled in by the editorial staff))
Revised: ((will be filled in by the editorial staff))
Published online: ((will be filled in by the editorial staff))

References

[1] C. Q. Yan, S. Barlow, Z. H. Wang, H. Yan, A. K. Y. Jen, S. R. Marder, X. W. Zhan, *Nat. Rev. Mater.* **2018**, *3*, 18003.

[2] P. Cheng, G. Li, X. W. Zhan, Y. Yang, *Nat. Photonics* **2018**, *12*, 131.

[3] G. Y. Zhang, J. B. Zhao, P. C. Y. Chow, K. Jiang, J. Q. Zhang, Z. L. Zhu, J. Zhang, F. Huang, H. Yan, *Chem. Rev.* **2018**, *118*, 3447.

[4] J. Hou, O. Inganäs, R. H. Friend, F. Gao, *Nat. Mater.* **2018**, *17*, 119-128.

[5] J. J. M. Halls, C. A. Walsh, N. C. Greenham, E. A. Marseglia, R. H. Friend, S. C. Moratti, A. B. Holmes, *Nature* **1995**, *376*, 498.

[6] G. Yu, J. Gao, J. C. Hummelen, F. Wudl, A. J. Heeger, *Science* **1995**, *270*, 1789.

[7] G. Li, R. Zhu, Y. Yang, *Nat. Photonics* **2012**, *6*, 153.

[8] Y. F. Li, *Acc. Chem. Res.* **2012**, *45*, 723.

[9] Y. Liu, J. Zhao, Z. Li, C. Mu, W. Ma, H. Hu, K. Jiang, H. Lin, H. Ade, H. Yan, *Nat. Commun.* **2014**, *5*, 5293.

[10] Z. C. He, B. Xiao, F. Liu, H. B. Wu, Y. L. Yang, S. Xiao, C. Wang, T. P. Russell, Y. Cao, *Nat. Photonics* **2015**, *9*, 174.

[11] P. Cheng, H. T. Bai, N. K. Zawacka, T. R. Andersen, W. Q. Liu, E. Bundgaard, M. Jorgensen, H. Chen, F. C. Krebs, X. W. Zhan, *Adv. Sci.* **2015**, *2*, 1500096.

[12] P. Cheng, X. W. Zhan, *Chem. Soc. Rev.* **2016**, *45*, 2544.

[13] L. X. Meng, Y. M. Zhang, X. J. Wan, C. X. Li, X. Zhang, Y. B. Wang, X. Ke, Z. Xiao, L. M. Ding, R. X. Xia, H. L. Yip, Y. Cao, Y. S. Chen, *Science* **2018**, *361*, 1094.

[14] J. Yuan, Y. Zhang, L. Zhou, G. Zhang, H.-L. Yip, T.-K. Lau, X. Lu, C. Zhu, H. Peng, P. A. Johnson, M. Leclerc, Y. Cao, J. Ulanski, Y. Li, Y. Zou, *Joule* **2019**, *3*, 1140.

[15] T. Liu, Z. H. Luo, Q. P. Fan, G. Y. Zhang, L. Zhang, W. Gao, X. Guo, W. Ma, M. J. Zhang, C. L. Yang, Y. F. Li, H. Yan, *Energy Environ. Sci.* **2018**, *11*, 3275.

[16] D. Baran, R. S. Ashraf, D. A. Hanifi, M. Abdelsamie, N. Gasparini, J. A. Rohr, S. Holliday, A. Wadsworth, S. Lockett, M. Neophytou, C. J. Emmott, J. Nelson, C. J. Brabec, A. Amassian, A. Salleo, T. Kirchartz, J. R. Durrant, I. McCulloch, *Nat. Mater.* **2017**, *16*, 363.

[17] S. Holliday, R. S. Ashraf, A. Wadsworth, D. Baran, S. A. Yousaf, C. B. Nielsen, C. H. Tan, S. D. Dimitrov, Z. Shang, N. Gasparini, M. Alamoudi, F. Laquai, C. J. Brabec, A. Salleo, J. R. Durrant, I. McCulloch, *Nat. Commun.* **2016**,*7*,11585.

[18] X. Z. Che, Y. X. Li, Y. Qu, S. R. Forrest, *Nat. Energy* **2018**, *3*, 422.

[19] T. Liu, D. Meng, Y. H. Cai, X. B. Sun, Y. Li, L. J. Huo, F. Liu, Z. H. Wang, T. P. Russell, Y. M. Sun, *Adv. Sci.* **2016**, *3*, 1600117.

[20] M. Hao, T. Liu, Y. Xiao, L.-K. Ma, G. Zhang, C. Zhong, Z. Chen, Z. Luo, X. Lu, H. Yan, L. Wang, C. Yang, *Chem. Mater.* **2019**, *31*,1752.

[21] W. Wang, C. Yan, T. K. Lau, J. Wang, K. Liu, Y. Fan, X. Lu, X. Zhan, *Adv. Mater.* **2017**, *29*, 1701308.

[22] T. F. Li, S. X. Dai, Z. F. Ke, L. X. Yang, J. Y. Wang, C. Q. Yan, W. Ma, X. W. Zhan, *Adv. Mater.* **2018**, *30*,1705969.

[23] L. J. Zuo, X. L. Shi, S. B. Jo, Y. Liu, F. Lin, A. K. Y. Jen, *Adv. Mater.* **2018**, *30*, 1706816.

[24] Z. Yao, X. Liao, K. Gao, F. Lin, X. Xu, X. Shi, L. Zuo, F. Liu, Y. Chen, A. K. Y. Jen, *J. Am. Chem. Soc.* **2018**, *140*, 2054.

[25] W. Gao, T. Liu, C. Zhong, G. Zhang, Y. Zhang, R. Ming, L. Zhang, J. Xin, K. Wu, Y. Guo, W. Ma, H. Yan, Y. Liu, C. Yang, *ACS Energy Lett.* **2018**, *3*, 1760.

[26] Y. Lin, Q. He, F. Zhao, L. Huo, J. Mai, X. Lu, C. J. Su, T. Li, J. Wang, J. Zhu, Y. Sun, C. Wang, X. Zhan, *J. Am. Chem. Soc.* **2016**, *138*, 2973.

[27] P. Cheng, J. Y. Wang, Q. Q. Zhang, W. C. Huang, J. S. Zhu, R. Wang, S. Y. Chang, P. Y. Sun, L. Meng, H. X. Zhao, H. W. Cheng, T. Y. Huang, Y. Q. Liu, C. C. Wang, C. H. Zhu, W. You, X. W. Zhan, Y. Yang, *Adv. Mater.* **2018**, ***30***, 1801501.

[28] P. Cheng, R. Wang, J. S. Zhu, W. C. Huang, S. Y. Chang, L. Meng, P. Y. Sun, H. W. Cheng, M. Qin, C. H. Zhu, X. W. Zhan, Y. Yang, *Adv. Mater.* **2018**, *30*, 1705243.

[29] Y. Lin, J. Wang, Z. G. Zhang, H. Bai, Y. Li, D. Zhu, X. Zhan, *Adv. Mater.* **2015**, *27*, 1170.

[30] Q. P. Fan, W. Y. Su, Y. Wang, B. Guo, Y. F. Jiang, X. Guo, F. Liu, T. P. Russell, M. J. Zhang, Y. F. Li, *Sci. China Chem.* **2018**, *61*, 531.

[31] L. Y. Lu, T. Y. Zheng, Q. H. Wu, A. M. Schneider, D. L. Zhao, L. P. Yu, *Chem. Rev.* **2015**, *115*, 12666.

[32] Y. Y. Liang, Z. Xu, J. B. Xia, S. T. Tsai, Y. Wu, G. Li, C. Ray, L. P. Yu, *Adv. Mater.* **2010**, *22*, 135.

[33] S.-H. Liao, H.-J. Jhuo, Y.-S. Cheng, S.-A. Chen, *Adv. Mater.* **2013**, *25*, 4766.

[34] M. Li, K. Gao, X. Wan, Q. Zhang, B. Kan, R. Xia, F. Liu, X. Yang, H. Feng, W. Ni, Y. Wang, J. Peng, H. Zhang, Z. Liang, H.-L. Yip, X. Peng, Y. Cao, Y. Chen, *Nat. Photonics* **2016**, *11*, 85.

[35] W. Zhao, S. Li, H. Yao, S. Zhang, Y. Zhang, B. Yang, J. Hou, *J. Am. Chem. Soc.* **2017**, *139*, 7148.

[36] S. Zhang, Y. Qin, J. Zhu, J. Hou, *Adv. Mater.* **2018**, *30*, 1800868.

[37] B. B. Fan, X. Y. Du, F. Liu, W. K. Zhong, L. Ying, R. H. Xie, X. F. Tang, K. An, J. M. Xin, N. Li, W. Ma, C. J. Brabec, F. Huang, Y. Cao, *Nat. Energy* **2018**, *3*,1051.

[38] G. Li, W. H. Chang, Y. Yang, *Nat. Rev. Mater.* **2017**, *2*, 17043.

[39] D. Dang, D. Yu, E. Wang, *Adv. Mater.* **2019**, *31*, 1807019.

[40] T. Liu, W. Gao, G. Zhang, L. Zhang, J. Xin, W. Ma, C. Yang, H. Yan, C. Zhan, J. Yao, *Sol. RRL* **2019**, *3*, 1800376.

[41] T. Liu, L. J. Huo, S. Chandrabose, K. Chen, G. C. Han, F. Qi, X. Y. Meng, D. J. Xie, W. Ma, Y. P. Yi, J. M. Hodgkiss, F. Liu, J. Wang, C. L. Yang, Y. M. Sun, *Adv. Mater.* **2018**, *30*, 1707353.

[42] B. Kan, J. B. Zhang, F. Liu, X. J. Wan, C. X. Li, X. Ke, Y. C. Wang, H. R. Feng, Y. M. Zhang, G. K. Long, R. H. Friend, A. A. Bakulin, Y. S. Chen, *Adv. Mater.* **2018**, *30*, 1704904.

[43] J. Wang, W. Wang, X. Wang, Y. Wu, Q. Zhang, C. Yan, W. Ma, W. You, X. Zhan, *Adv. Mater.* **2017**, *29*, 1702125.

[44] J. Y. Wang, J. X. Zhang, Y. Q. Xiao, T. Xiao, R. Y. Zhu, C. Q. Yan, Y. Q. Fu, G. H. Lu, X. H. Lu, S. R. Marder, X. W. Zhan, *J. Am. Chem. Soc.* **2018**, *140*, 9140.

[45] W. Gao, T. Liu, J. Li, Y. Xiao, G. Zhang, Y. Chen, C. Zhong, X. Lu, H. Yan, C. Yang, *J. Mater. Chem. A* **2019**, ***7***, 11053.

[46] Y. Z. Chen, T. Liu, H. W. Hu, T. X. Ma, J. Y. L. Lai, J. Q. Zhang, H. Ade, H. Yan, *Adv. Energy Mater.* **2018**, *8*, 1801203.

[47] H. F. Yao, Y. Cui, R. N. Yu, B. W. Gao, H. Zhang, J. H. Hou, *Angew. Chem.-Int. Edit.* **2017**, *56*, 3045-3049.

[48] Y. C. Wang, Y. B. Wang, B. Kan, X. Ke, X. J. Wan, C. X. Li, Y. S. Chen, *Adv. Energy Mater.* **2018**, *8*, 1802021.

[49] W. Zhao, D. Qian, S. Zhang, S. Li, O. Inganas, F. Gao, J. Hou, *Adv. Mater.* **2016**, *28*, 4734.

[50] Z. Tan, S. Li, F. Wang, D. Qian, J. Lin, J. Hou, Y. Li, *Sci. Rep.* **2014**, *4*, 4691.

[51] V. D. Mihailetchi, L. J. A. Koster, J. C. Hummelen, P. W. M. Blom, *Phys. Rev. Lett.* **2004**, *93*, 216601.

[52] H. Yin, J. K. W. Ho, S. H. Cheung, R. J. Yan, K. L. Chiu, X. T. Hao, S. K. So, *J. Mater. Chem. A* **2018**, *6*, 8579.

[53] H. Yin, P. Q. Bi, S. H. Cheung, W. L. Cheng, K. L. Chiu, C. H. Y. Ho, H. W. Li, S. W. Tsang, X. T. Hao, S. K. So, *Sol. RRL* ***2018***, 2, 1700239.

[54] J. Mai, Y. Xiao, G. Zhou, J. Wang, J. Zhu, N. Zhao, X. Zhan, X. Lu, *Adv. Mater.* **2018**, *30*, 1802888.

[55] J. Mai, T.-K. Lau, J. Li, S.-H. Peng, C.-S. Hsu, U. S. Jeng, J. Zeng, N. Zhao, X. Xiao, X. Lu, *Chem. Mater.* **2016**, *28*, 6186.

TOC

We designed three novel low-bangap FREAs, BPIC, BPIC-2Cl and BPIC-4Cl, based on a heptacyclic core using phenyl substituted BDT as the central unit, end-capped with INCN, mono-chlorinated INCN, and di-chlorinated INCN moieties, respectively, and investigated the effects of chlorination on optical and electronic potentials of these molecules, as well as morphology and photovoltaic performance of organic solar cells.